Small strain stiffness anisotropy of natural sedimentary clays - review and a model

David Mašín and Josef Rott
Charles University in Prague

corresponence address:
David Mašín
Charles University in Prague
Faculty of Science
Albertov 6
12843 Prague 2, Czech Republic
E-mail: masin@natur.cuni.cz
Tel: +420-2-2195 1552, Fax: +420-2-2195 1556

August 13, 2013

Abstract

Very small strain stiffness anisotropy of sedimentary clays is investigated. First, a general formulation of transversely isotropic elastic model is summarised, followed by a description of its complete parameter identification using transversal and longitudinal wave velocity measurements. Then, an extensive experimental database from the literature is reviewed. A number of general trends in the observed behaviour is identified, based on which a model is developed describing the dependency of the ratio of in-plane and transversal very small strain shear moduli on the stress state and overconsolidation ratio. Subsequently, an empirical relation between the ratios of shear moduli and Young moduli is quantified. The most problematic tend to be the evaluation of Poisson ratios and evolution of stiffness anisotropy under general stress conditions. These issues remain to be investigated experimentally in future work.

Keywords: anisotropy; clay; elasticity; stiffness; constitutive modelling

1 Introduction

Anisotropy of the very small strain stiffness[1] of fine grained soils is a complicated subject matter, with a number of issues which remain to be clarified. Yet, it has a pronounced effect on numerical predictions of geotechnical structures, as demonstrated for example in [1, 16, 9, 13]. In this paper, we attempt to develop a heuristic model for the very small strain stiffness anisotropy of sedimentary clays, which is based on an extensive literature review of experimental data. The model brings new insights into the stiffness anisotropy of clays and identifies the most problematic areas, which should be the scope of further research. The primary goal of this paper is to develop a formulation to be used as a very-small-strain component of more advanced constitutive models for clays, such as the hypoplastic model by Mašín [29, 30]. Large strain and strength anisotropy may also be considered in soil constitutive modelling [42, 35], it is however out of the scope of the present paper.

In the following, we will distinguish two sources of clay anisotropy. *Inherent* anisotropy, which is caused by the prevalent orientation of platy clay particles and *stress-induced* anisotropy, caused by the anisotropy of the stress state. The inherent anisotropy is typically transversely isotropic, as it is formed during the deposition and subsequent consolidation and diagenetic processes, which mostly take place under oedometric conditions. Contrary, the stress-induced anisotropy is under general stress conditions not bound to transverse isotropy. In this work,

[1] The notion of very small strain stiffness represents stiffness measured in the strain range approximately below 10^{-5}. In this strain range, the stiffness is approximately constant, independent of the strain magnitude [2, 7, 6].

we only study soils under axisymmetric stress conditions with the axis of symmetry coinciding with the axis of inherent transverse isotropy. Under general stress conditions the anisotropic soil properties become extremely complex, as they are no-more bound by the five-parameter transversely isotropic elasticity; practically no data are available to date for their evaluation.

2 Formulation of transversely isotropic elastic model

2.1 General stiffness matrix formulation

Let us restrict our attention to linear kinematics and denote Cauchy stress rate by $\dot{\boldsymbol{\sigma}}$ and the strain rate by $\dot{\boldsymbol{\epsilon}}$. Stiffness matrix $\boldsymbol{\mathcal{M}}$ of transversely isotropic material, representing linear mapping between the strain and stress rates

$$\dot{\boldsymbol{\sigma}} = \boldsymbol{\mathcal{M}} : \dot{\boldsymbol{\epsilon}} \tag{1}$$

may be formulated using representation theorems for transversely isotropic tensor function of a strain tensor an unit vector as [46, 27]

$$\boldsymbol{\mathcal{M}} = \frac{1}{2} a_1 \mathbf{1} \circ \mathbf{1} + a_2 \mathbf{1} \otimes \mathbf{1} + a_3 \left(\boldsymbol{p} \otimes \mathbf{1} + \mathbf{1} \otimes \boldsymbol{p} \right) + a_4 \boldsymbol{p} \circ \mathbf{1} + a_5 \boldsymbol{p} \otimes \boldsymbol{p} \tag{2}$$

where the tensor products represented by "$\circ$" and "$\otimes$" are defined by

$$(\boldsymbol{p} \otimes \mathbf{1})_{ijkl} = p_{ij} 1_{kl} \qquad (\boldsymbol{p} \circ \mathbf{1})_{ijkl} = \frac{1}{2} \left(p_{ik} 1_{jl} + p_{il} 1_{jk} + p_{jl} 1_{ik} + p_{jk} 1_{il} \right) \tag{3}$$

$\mathbf{1}$ is the second-order unit tensor. The tensor p_{ij} is defined as $p_{ij} = n_i n_j$, where n_i is a unit vector normal to the plane of symmetry (in sedimentary soils this vector typically represents the vertical direction). a_1 to a_5 in Eq. (2) represent five material constants. Possible approach to their determination is summarised later in Sec. 3.

2.2 Engineering formulation

The constants a_1 to a_5 may be expressed in terms of the engineering variables G_{tp}, G_{pt}, G_{pp}, E_t, E_p, ν_{tp}, ν_{pt} and ν_{pp} as [27]

$$a_1 = 2G_{pp} \tag{4}$$

$$a_2 = K\frac{E_p}{E_t}\left(\nu_{pp} + \nu_{tp}\nu_{pt}\right) \tag{5}$$

$$a_3 = K\nu_{pt}\left(1 + \nu_{pp} - \frac{\nu_{pp}}{\nu_{tp}} - \nu_{pt}\right) \tag{6}$$

$$a_4 = 2\left(G_{tp} - G_{pp}\right) \tag{7}$$

$$a_5 = K\left[\frac{E_p}{E_t}\left(1 - \nu_{tp}\nu_{pt}\right) + 1 - \nu_{pp}^2 - 2\nu_{pt}\left(1 + \nu_{pp}\right)\right] - 4G_{tp} \tag{8}$$

where

$$K = \frac{E_t}{\left(1 + \nu_{pp}\right)\left(1 - \nu_{pp} - 2\nu_{tp}\nu_{pt}\right)} \tag{9}$$

In Eqs. (4) and (9) subscript "$_p$" denotes direction within the plane of isotropy (typically horizontal direction), subscript "$_t$" denotes direction transverse to the plane of isotropy (typically vertical direction), G_{ij} are shear moduli, E_i are Young moduli and ν_{ij} are Poisson ratios. Some of the engineering constants are inter-related. The existence of the plane of isotropy implies

$$G_{pp} = \frac{E_p}{2\left(1 + \nu_{pp}\right)} \tag{10}$$

the requirement of the stiffness matrix symmetry leads to [41, 38]

$$\frac{\nu_{tp}}{E_t} = \frac{\nu_{pt}}{E_p} \tag{11}$$

and transverse isotropy assumption itself implies that

$$G_{tp} = G_{pt} \tag{12}$$

The engineering formulation is often expressed in the Voigt notation. In this notation, the stress and strain rate tensors are written in the coordinate system aligned with the axes of symmetry using six-component vectors:

$$\dot{\boldsymbol{\sigma}} = \begin{bmatrix} \dot{\sigma}_{11} \\ \dot{\sigma}_{22} \\ \dot{\sigma}_{33} \\ \dot{\sigma}_{23} \\ \dot{\sigma}_{13} \\ \dot{\sigma}_{12} \end{bmatrix} \qquad \dot{\boldsymbol{\epsilon}} = \begin{bmatrix} \dot{\epsilon}_{11} \\ \dot{\epsilon}_{22} \\ \dot{\epsilon}_{33} \\ \dot{\gamma}_{23} = 2\dot{\epsilon}_{23} \\ \dot{\gamma}_{13} = 2\dot{\epsilon}_{13} \\ \dot{\gamma}_{12} = 2\dot{\epsilon}_{12} \end{bmatrix} \tag{13}$$

with the direction "$_1$" being normal to the plane of symmetry. The compliance matrix $\boldsymbol{\mathcal{C}} = \boldsymbol{\mathcal{M}}^{-1}$ then takes the form familiar in soil mechanics science

$$\boldsymbol{\mathcal{C}} = \begin{bmatrix} \frac{1}{E_t} & -\frac{\nu_{pt}}{E_p} & -\frac{\nu_{pt}}{E_p} & \cdot & \cdot & \cdot \\ -\frac{\nu_{tp}}{E_t} & \frac{1}{E_p} & -\frac{\nu_{pp}}{E_p} & \cdot & \cdot & \cdot \\ -\frac{\nu_{tp}}{E_t} & -\frac{\nu_{pp}}{E_p} & \frac{1}{E_p} & \cdot & \cdot & \cdot \\ \cdot & \cdot & \cdot & \frac{1}{G_{pp}} & \cdot & \cdot \\ \cdot & \cdot & \cdot & \cdot & \frac{1}{G_{pt}} & \cdot \\ \cdot & \cdot & \cdot & \cdot & \cdot & \frac{1}{G_{tp}} \end{bmatrix} \tag{14}$$

The stiffness matrix can in the same notation be expressed formally as [14]

$$\boldsymbol{\mathcal{M}} = \begin{bmatrix} A & B & B & \cdot & \cdot & \cdot \\ B & C & D & \cdot & \cdot & \cdot \\ B & D & C & \cdot & \cdot & \cdot \\ \cdot & \cdot & \cdot & \frac{C-D}{2} & \cdot & \cdot \\ \cdot & \cdot & \cdot & \cdot & E & \cdot \\ \cdot & \cdot & \cdot & \cdot & \cdot & E \end{bmatrix} \tag{15}$$

and more specifically by

$$\boldsymbol{\mathcal{M}} = \begin{bmatrix} K\left(1-\nu_{pp}^2\right) & K\nu_{pt}\left(1+\nu_{pp}\right) & K\nu_{pt}\left(1+\nu_{pp}\right) & \cdot & \cdot & \cdot \\ K\nu_{pt}\left(1+\nu_{pp}\right) & K\frac{E_p}{E_t}\left(1-\nu_{tp}\nu_{pt}\right) & K\frac{E_p}{E_t}\left(\nu_{pp}+\nu_{tp}\nu_{pt}\right) & \cdot & \cdot & \cdot \\ K\nu_{pt}\left(1+\nu_{pp}\right) & K\frac{E_p}{E_t}\left(\nu_{pp}+\nu_{tp}\nu_{pt}\right) & K\frac{E_p}{E_t}\left(1-\nu_{tp}\nu_{pt}\right) & \cdot & \cdot & \cdot \\ \cdot & \cdot & \cdot & G_{pp} & \cdot & \cdot \\ \cdot & \cdot & \cdot & \cdot & G_{pt} & \cdot \\ \cdot & \cdot & \cdot & \cdot & \cdot & G_{tp} \end{bmatrix} \tag{16}$$

with K given by (9). Eq. (16) is equivalent to Eq. (2) with $n = [1, 0, 0]$. An advantage of Eq. (2) is that any (even inclined) plane of symmetry can be modelled easily. This enables, as an example, to model strata which were rotated or folded by post-depositional geological processes.

2.3 Coefficients of anisotropy

To aid the evaluation of experimental data, the anisotropic elasticity models will be formulated in terms of so-called *coefficients of anisotropy*. These coefficients represent ratios of shear and Young moduli and Poisson ratios and they will be denoted as α, following the landmark work by Graham and Houlsby [14]. We define the following three coefficients as

$$\alpha_G = \frac{G_{pp}}{G_{tp}} \tag{17}$$

$$\alpha_E = \frac{E_p}{E_t} \tag{18}$$

$$\alpha_\nu = \frac{\nu_{pp}}{\nu_{tp}} \tag{19}$$

and the following two anisotropy exponents x_{GE} and $x_{G\nu}$ as

$$\alpha_G = \alpha_E^{x_{GE}} \tag{20}$$

$$\alpha_G = \alpha_\nu^{x_{G\nu}} \tag{21}$$

$$\tag{22}$$

A complete transversely isotropic elastic model can then be defined using two elastic constants (for example, G_{tp} and ν_{pp}), anisotropy coefficient α_G and two anisotropy exponents x_{GE} and $x_{G\nu}$. This formulation will be adopted in this paper.

At this point it is important to point out that the model formulation using parameters G_{tp}, ν_{pp}, α_G, α_E and α_ν represents fully general transversely elastic model. Different approaches are then possible to represent the material parameters. By example, one can specify the cross-dependency of G_{tp}, ν_{pp}, α_G, α_E and α_ν such that the model is consistent with the second law of thermodynamics (the model is hyperelastic). Another, phenomenological approach, adopts stiffness measurements to specify the material constants experimentally. In this work we adopt the latter approach, while we point out that the hyperelasticity model may be developed at the later stage with the aid of the data presented in this paper.

The formulation using coefficients G_{tp}, ν_{pp}, α_G, x_{GE} and $x_{G\nu}$ is no more fully general, as it is not possible to vary α_E and α_ν independently of α_G (α_ν cannot be negative, while this is a theoretically admissible case). We adopt this form, however, as it aids the development of empirically based model.

3 Measurement of the anisotropy constants by means of wave propagation

Soil behaviour is elastic in the very small strain range only and for this reason the determination of the elastic material constants is rather complicated. Two different experimental procedures may be adopted. The first adopts static loading tests at variable boundary conditions with local measurements of sample deformation [2]. This approach is often biased by insufficient accuracy of experimental devices and high experimental scatter in the very small strain range. The second approach uses the fact that the wave propagation velocities depend on the soil stiffness. We will focus on the latter approach, although it is noted that also these measurements are not straightforward [15].

Among different methods of wave velocity measurements the most popular is probably measurement by bender elements [45]. A comprehensive setup, which allows to generate transversal waves (S-waves) as well as longitudinal waves (P-waves) has been presented by Ezaoui and Di Benedetto [8]. For determination of all the five elastic constants, five wave velocity measurements are needed. The parameters A, B, C, D and E from Eq. (15) can be related to wave velocities by (from [28])

$$C = \rho V_P^2(90^\circ) \tag{23}$$

$$D = C - 2\rho V_{SH}^2(90^\circ) \tag{24}$$

$$A = \rho V_P^2(0^\circ) \tag{25}$$

$$E = \rho V_{SH}^2(0^\circ) \tag{26}$$

$$B = -E + \sqrt{4\rho^2 V_P^4(45^\circ) - 2\rho V_P^2(45^\circ)\left(C + A + 2E\right) + \left(C + E\right)\left(A + E\right)} \tag{27}$$

The elastic constants adopted in this paper can be obtained by manipulation with (15) and (16):

$$G_{tp} = E \tag{28}$$

$$\alpha_G = \frac{C - D}{2E} \tag{29}$$

$$\nu_{pp} = \frac{AD - B^2}{AC - B^2} \tag{30}$$

$$\alpha_\nu = \frac{C + D}{B}\nu_{pp} \tag{31}$$

$$\alpha_E = \frac{B\alpha_\nu^2 - C\alpha_\nu \nu_{pp}\left(1 + \nu_{pp}\right)}{B\nu_{pp}^2} \tag{32}$$

In Eqs. (23) to (27), V_{SH} represent velocity of propagation of S-wave and V_P represent velocity of propagation of the P-wave. The angle in bracket represents the angle between wave propagation direction and the axis of symmetry (direction normal to the plane of isotropy).

Measurement of all elastic constants using wave propagation technique is possible, however certainly not routine. While measurements of V_{SH} become more affordable at present days, measurement of $V_P(0°)$ and $V_P(90°)$ is still relatively rarely reported in the literature [8] and, in fact, the authors are not aware of published measurements of $V_P(45°)$ on soil samples. To this reason, uncommon types of experiments are often replaced by empirical formulations: every empirical expression reduces the necessary number of experiments to characterise the small strain stiffness by one, while obviously introducing certain ambiguity into the calibration. Development and evaluation of such empirical expressions using experimental data available to date in the literature is the primary aim of this paper.

4 Existing anisotropy models

A complete description of transverse isotropic properties of natural soils is remarkably complicated. Adopting the five-parameter G_{tp}, ν_{pp}, α_G, x_{GE}, $x_{G\nu}$ formulation from Sec. 2.3, the following issues arise when defining the transverse isotropic elastic behaviour of soils:

1. The very small strain stiffness shear and Young moduli depend on material state, measured by the effective stress tensor and void ratio. A number of models have been proposed and evaluated describing this dependency by different authors (see [50, 49, 18, 37, 34, 44, 43]). In this paper, we will focus on material anisotropy measured by α_G, x_{GE} and $x_{G\nu}$; the dependency of the primary elastic constant G_{tp} and ν_{pp} on material state is out of the paper scope and the readers are referred to the above cited publications.

2. Anisotropy evolves during loading process and thus the coefficient α_G depends on soil state. This dependency has been studied experimentally by different researchers, but to the author's knowledge, no general model for the anisotropy evolution of sedimentary clays has been proposed as yet. Such a model is one of the objectives of this paper.

3. The anisotropy exponents x_{GE} and $x_{G\nu}$ may also depend on soil state. The experimental database is scarce, however, and many authors adopt empirical equations for x_{GE} and $x_{G\nu}$ instead of their experimental determination. The most popular model is due to

Graham and Houlsby [14], who postulated

$$x_{GE} = 0.5 \tag{33}$$

$$x_{G\nu} = 1 \tag{34}$$

This model was, however, developed without a direct experimental support and, to the author's knowledge, its adequacy has not been studied systematically as yet using the experimental database available in the literature. Evaluation of the empirical equations for x_{GE} and $x_{G\nu}$ represent the second objective of this paper.

The experimental data used for development of the models are summarised in Sec. 5 and 6.

5 Experimental evidence for α_G and its evolution with soil state

The aim of this paper is to study stiffness anisotropy of sedimentary clays. Apart from the behaviour of natural stiff and soft clays, however, we review also the data on reconstituted clays. They give us an insight into the possible evolution of anisotropy during post-depositional one-dimensional compression. The experimental database adopted, including basic soil properties and experimental procedures, is summarised in Tabs. 1-4.

Each experimental dataset is in Tables 1-4 described by a label used in all subsequent graphs. Column "material details" gives some information on the soil provided by the authors, such as Atterberg limits, age, percentage of fines (CF), etc. Column "stiffness measurement" provides information on the experimental device, where TX denotes triaxial apparatus and OED denotes oedometric apparatus. Column "one sample" informs whether the experimental dataset represents one sample loaded to various stress levels (label "one") or multiple samples obtained from different sampling depths reconsolidated to different (typically *in-situ*) stresses (label "many"). η is defined as the ratio $\eta = q/p$, where q is deviatoric stress and p is mean stress. OCR is overconsolidation ratio.

Some assumptions had to be made while evaluating the literature data. In particular, it was often necessary to calculate the mean stress p from the known value of vertical stress σ_v. For this purpose, K_0 was estimated by Mayne and Kulhawy [31] empirical relationship

$$K_0 = (1 - \sin\varphi_c)\, OCR^{\sin\varphi_c} \tag{35}$$

where OCR represents overconsolidation ratio and φ_c is critical state friction angle, assumed

Table 1: Details on experimental data used in the evaluation, part 1 (reconstituted clays).

graph label	source	material	material details	test type	stiffness measurement	one sample
Lucera M RK_0	Mitarionna et al. [32]	reconst.	Lucera clay, Italy. $w_L = 48\%$, IP=25%, CF=43%, A=0.51	K_0 consolidation (η controlled)	TX, vert. & hor. bender el.	one
Bangkok K RK_0	Kawaguchi et al. [19]	reconst.	Bangkok clay. $w_L = 81.2\%$	K_0 consolidation	TX, vert. & hor. bender el.	one
Pisa K RK_0	Kawaguchi et al. [19]	reconst.	Pisa clay, from the tower of Pisa site, $w_L = 89.3\%$	K_0 consolidation	TX, vert. & hor. bender el.	one
Kobe K RK_0	Kawaguchi et al. [19]	reconst.	Kobe airport clay, Pleistocene, $w_L = 59\%$	K_0 consolidation	TX, vert. & hor. bender el.	one
Taipei F RK_0	Fu-Chen [10]	reconst.	Taipei clay, site TNEC. depth 9 to 27 m, silty clay, $w_L = 43\%$, $I_P = 20\%$ (from [21])	K_0 consolidation	TX, vert. & hor. bender el.	one
Kaolin C RK_0	Choo et al. [5]	reconst.	Kaolin clay, $w_L = 53\%$, $I_P = 20\%$	K_0 consolidation	TX, vert. & hor. bender el.	one
Gault P RI	Pennington et al. [37]	reconst.	Gault clay, Madingley near Cambridge. Late Cretaceous. High plasticity silty clay, 30% $CaCO_3$	Isotrop. cons of K_0 preconsolidated sample ($\sigma_v = 165$ kPa)	TX, vert. & hor. bender el.	one
London J RI	Jovičić and Coop [18]	reconst.	London clay. Slightly calcareous silty to very silty clay, Eocene age, marine. Illite and smectite dominates in central London. $w = 22-27\%$, $w_L = 60-70\%$, $I_P = 35-40\%$ (from [11])	Isotrop. cons (400 kPa) of K_0 preconsolidated sample ($\sigma_v = 1500$ kPa)	TX, vert. bender el., oriented samples	one
NSF Y RI	Yamashita et al. [51]	reconst.	NSF clay, $w_L = 58\%$, $I_P = 30\%$	Isotrop. cons of K_0 preconsolidated sample ($\sigma_v = 150$ kPa)	TX, vert. & hor. bender el.	one
Kaolin K RI	Kuwano et al. [22]	reconst.	Kaolin, speswhite fine china clay, $w_L = 62\%$, $I_P = 30\%$	Isotrop. cons of K_0 preconsolidated sample ($\sigma_v = 100$ kPa)	TX, vert. & hor. bender el.	one
Boom P R$K_0 > 1$	Piriyakul [39]	reconst.	Boom clay, Belgium. Middle Oligocene (35 Ma), marine, $w_L = 65\%$, $I_P = 41\%$. 50% clay, 50% silt.	Consolidometer to $w = 24\%$ of natural sample. Then $K_0 = 2$ loading and unloading	TX, vert. & hor. bender el. Vert. and horiz. Hall effect transducers.	one

graph label	source	material	material details	test type	stiffness measurement	one sample
Panigaglia J NK_0	Jamiolkowski et al. [17]	soft, nat.	Panigaglia clay. Recent marine deposit, Very soft high plasticity slightly organic silty clay not more then 1000 years old, OCR=1 to 1.1, depth 19.3m. w_L = 71%, IP=44%, CF=40%	K_0 loading to 1000 kPa and unloading to 37 kPa	OED, vert. & hor. bender el., K_0 measurement.	one
Pisa J NK_0	Jamiolkowski et al. [17]	soft, nat.	Pisa clay. Soft, medium-high plasticity silty clay, upper Pleistocene. OCR=1.5 to 2 (due to aging). depth 13m. $w_L = 35 - 77\%$, IP=23-46%, CF=30-70%	K_0 loading to 626 kPa and unloading to 31 kPa	OED, vert. & hor. bender el., K_0 measurement.	one
Chicago C NK_0	Cho and Finno [4]	soft, nat.	Chicago glacial clay (till), Evanson, depth 8.3m. Distinct sheets during local glacier advances and retreats during Wisconsin stage. Small overconsolidation.	K_0 reconsolidation to the *in-situ* stress	OED, vert. & hor. bender el.	many
Pietrafitta C NK_0	Callisto and Rampello [3]	medium stiff, nat.	Pietrafitta, South of Perugia, Italy. Lacustrine, early Pleistocene, high plasticity silty clay, depth 39 m, w_L = 96%, IP=61%, CF=84%	Const. η consol. up to p = 650 kPa (preceded by isotropic reconsolidation to 250 kPa and const. p to $\eta = 0.5$)	TX, vert. & hor. bender el.	one
Taipei F NK_0	Fu-Chen [10]	soft, nat.	see "Taipei F RK_0"	K_0 reconsolidation to the *in-situ* stress state (100-250 kPa)	TX, vert. & hor. bender el.	many

Table 2: Details on experimental data used in the evaluation, part 2 (natural soft clays).

Table 3: Details on experimental data used in the evaluation, part 3 (natural soft clays, cont'd.).

graph label	source	material	material details	test type	stiffness measurement	one sample
Bangkok T NK_0	Teachavorasinskun and Lukkanaprasit [47]	soft, nat.	soft Bangkok clay, center of Bangkok, $w_L = 80\%$, $I_P = 55\%$, depth 7-15m	K_0 cons.	OED, vert. & hor. bender el.	one
Pisa K NK_0	Kawaguchi et al. [19]	soft, nat.	see "Pisa K RK_0", depth 18m	K_0 cons. and unload	TX, vert. & hor. bender el.	one
Bangkok K NK_0	Kawaguchi et al. [19]	soft, nat.	see "Bangkok K RK_0", depth 10m	K_0 cons. to the *in-situ* state	TX, vert. & hor. bender el.	one
Kobe K NK_0	Kawaguchi et al. [19]	soft, nat.	see "Kobe K RK_0", depth 95m	K_0 cons. to the *in-situ* state	TX, vert. & hor. bender el.	one
Shanghai L NI	, Li et al. [25], Li [24], Ng et al. [33]	soft, nat.	Longhua Station of Shanghai Metro Line 7, depth 8.5 m, greyish soft clay with very fine sand partings, OCR=1.1, $w_L = 51\%$, $I_P = 25\%$,	Isotropic consolidation up to 400 kPa	TX, vert. & hor. bender el., prismatic sample	one
Bangkok R NI	Ratananikom et al. [40]	soft, nat.	see "Bangkok K RK_0", depth 12.9-13.1m	Isotrop. cons. to p=100 kPa	TX, vert. bender el., oriented samples	one
Burswood L NI-unl	Landon and DeGroot[23]	soft, nat.	Burswood clay, Perth, Western Australia. Medium sensitivity soft clay, numerous silt lenses. OCR 1.8-1.4	Unloaded samples extracted from borehole, residual suction	portable bender elements	many
OnsoyL NIunl	Landon and DeGroot[23]	soft, nat.	Onsøy clay, soft, normally to lightly overconsolidated, high plasticity clay. OCR averages 1.4. Sensitivity 4 to 9.	Unloaded samples extracted from borehole, residual suction	portable bender elements	many

Table 4: Details on experimental data used in the evaluation, part 4 (natural stiff clays).

graph label	source	material	material details	test type	stiffness measurement	one sample
London N N$K_0 > 1$	Nishimura [36]	stiff, nat.	London clay, see "London J RI"	reconsolidation to the estimated *in-situ* state with $K_0 > 1$	TX, vert. & hor. bender el.	many
London G N$K_0 > 1$	Gasparre [11], Gasparre et al. [12]	stiff, nat.	London clay, see "London J RI"	reconsolidation to the estimated *in-situ* state with $K_0 > 1$	TX, vert. & hor. bender el.	many
London N NI	Nishimura [36]	stiff, nat.	London clay, see "London J RI"	isotropic reconsolidation *in-situ* mean stress	TX, vert. & hor. bender el.	many
Boom P N$K_0 > 1$	Piriyakul [39]	stiff, nat.	see "Boom P R$K_0 > 1$", depth 8 m	$K_0 = 2$ loading and unloading	TX, vert. & hor. bender el., horiz. and vert. hall effect transducers	one
Boom P NI	Piriyakul [39]	stiff, nat.	see "Boom P R$K_0 > 1$", depth 8 m	isotrop. cons to three different stresses	TX, vert. & hor. bender el.	one
Gault P N$K_0 > 1$	Pennington et al. [37]	stiff, nat.	see "Gault P RI", depth 8 m	Isotropic consolidation up to the *in-situ* vertical stress, then increase of σ_h till $K_0 = 2.1$	TX, vert. & hor. bender el.	one
Gault L N$K_0 > 1$	Lings et al. [26]	stiff, nat.	see "Gault P RI", depth 6-8 m	Like "Gault P N$K_0 > 1$" up to $K_0 = 2$, then drained excursions for other elastic param.	TX, vert. & hor. bender el., horiz. and vert. hall effect transducers	one
London J NI	Jovičić and Coop [18]	stiff, nat.	London clay, see "London J RI"	Isotrop. cons (400 kPa) to the *in-situ* mean stress	TX, vert. bender el., oriented samples	many
Gault Y NI	Yimsiri and Soga [52]	stiff, nat.	Gault clay, Eversden, Cambridge. depth 14-16m. $w_L = 74\%$, $I_P = 43\%$	Isotropic cons. 240-250 kPa	TX, oriented specimens, vertical bend. el., axial LDTs, radial proximity trans.	one
London Y NI	Yimsiri and Soga [52]	stiff, nat.	London clay. depth 12-23m. see "London J RI"	Isotropic cons. 240-320 kPa	see "Gault Y NI"	one
Boston L NIunl	Landon and DeGroot[23]	stiff, nat.	Boston blue clay, Newbury (55km north of Boston). Glacial marine deposit, firm to stiff. $w_L = 34\%$, $I_P = 17\%$	Unloaded samples extracted from borehole, residual suction	portable bender elements	many

as $\varphi_c = 20^\circ$ if not known for the particular soil type.

5.1 Evolution of α_G of reconstituted clays

We first start with the evolution of stiffness anisotropy during loading of reconstituted clays. It is reasonable to assume that these soils, prepared from slurry at a water content higher than the liquid limit, have initially isotropic structure. Development of stiffness anisotropy during oedometric compression is shown in Fig. 1. Apart from the Lucera clay, which posses very low degree of anisotropy throughout the loading process, all the samples show consistent increase of α_G during oedometric compression. Virgin one-dimensional loading of soft clayey soil thus influences the degree of anisotropy in a substantial way.

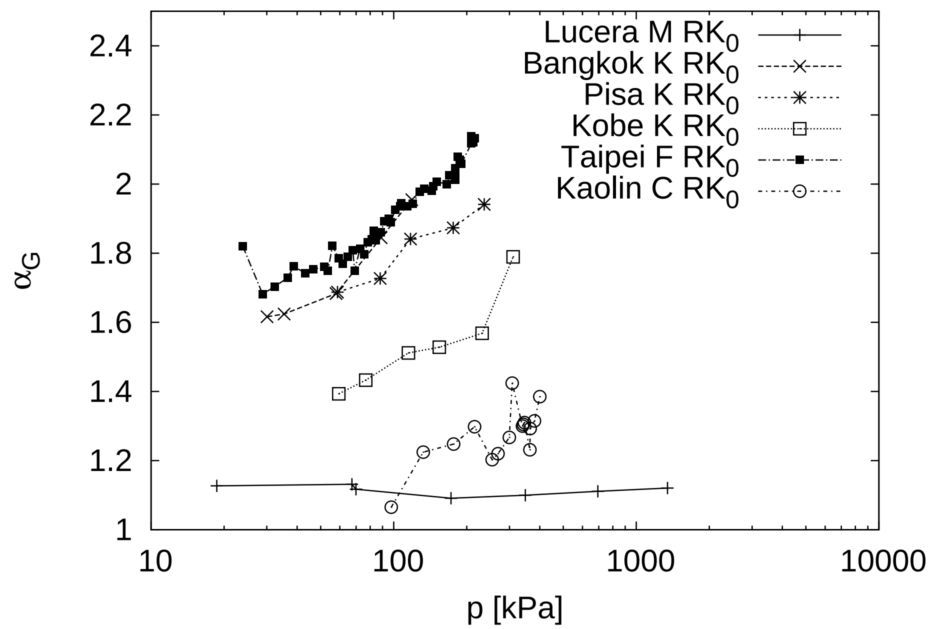

Figure 1: Development of stiffness anisotropy during virgin oedometric loading of reconstituted clays (for data sources see Tab. 1).

Figure 2 shows the development of α_G in reconstituted samples compressed by isotropic stresses after one-dimensional preconsolidation in a consolidometer. The sample of London clay has been oedometrically preconsolidated to high stress $\sigma_v = 1500$ kPa, whereas the other samples to lower vertical stresses between 100 and 200 kPa, see Tab. 1. Unlike virgin K_0 loading, the isotropic loading of preconsolidated samples has only minor effect on the α_G evolution. In fact, only the London clay sample, which has been loaded to a high mean stress of 3 MPa, shows a mild decrease of stiffness anisotropy starting approximately at the preconsolidation stress level. These data demonstrate that an inherent stiffness anisotropy created by virgin loading cannot be erased easily during the subsequent loading process.

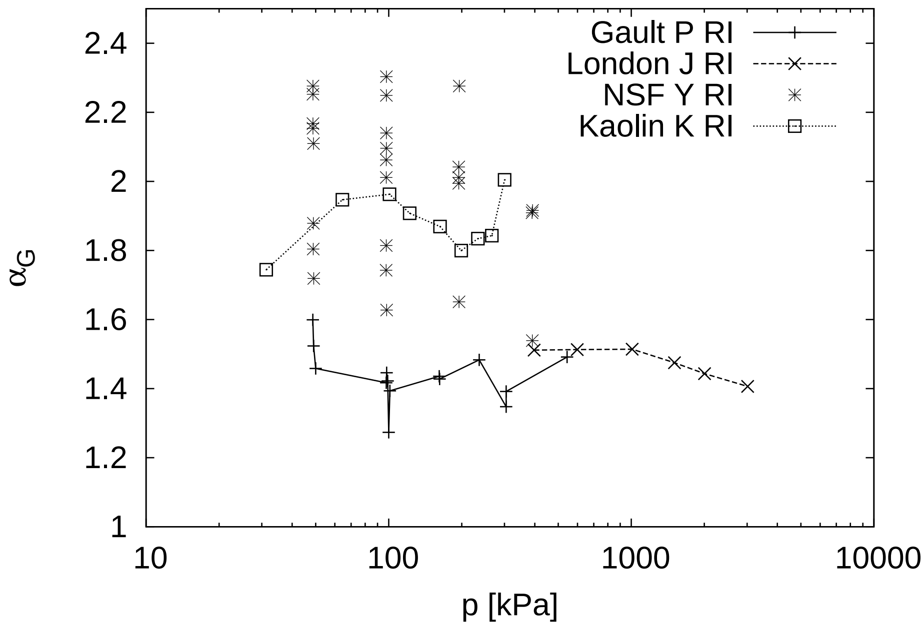

Figure 2: Development of stiffness anisotropy during isotropic loading of K_0 preconsolidated reconstituted clays (for data sources see Tab. 1).

In principle, even more drastic effect on an inherent anisotropy degradation should have loading under conditions of $K_0 > 1$ ($\eta < 0$). Such a data on reconstituted Boom clay present Piriyakul [39] (Fig. 3). Loading took place at $K_0 = 2$. As expected, α_G decreases faster then during isotropic compression. Loading from 100 kPa to 400 kPa was still not capable of complete destruction of soil anisotropic fabric, however.

Figure 3 shows also results of $K_0 = 2$ unloading test. Clearly, inherent soil anisotropy degrades during loading only. Unloading at constant K_0 (constant η), or loading of overconsolidated sample (see "London J RI" data in Fig. 2 below the preconsolidation stress level) does not modify the stiffness anisotropy in any way.

5.2 Evolution of α_G of soft sedimentary clays

Let us now study the anisotropy evolution during oedometric loading of soft natural clays (Fig. 4). The picture is now less clear than during virgin loading of reconstituted soils. Consistently with the reconstituted soil behaviour, some tests show an increase of soil anisotropy during

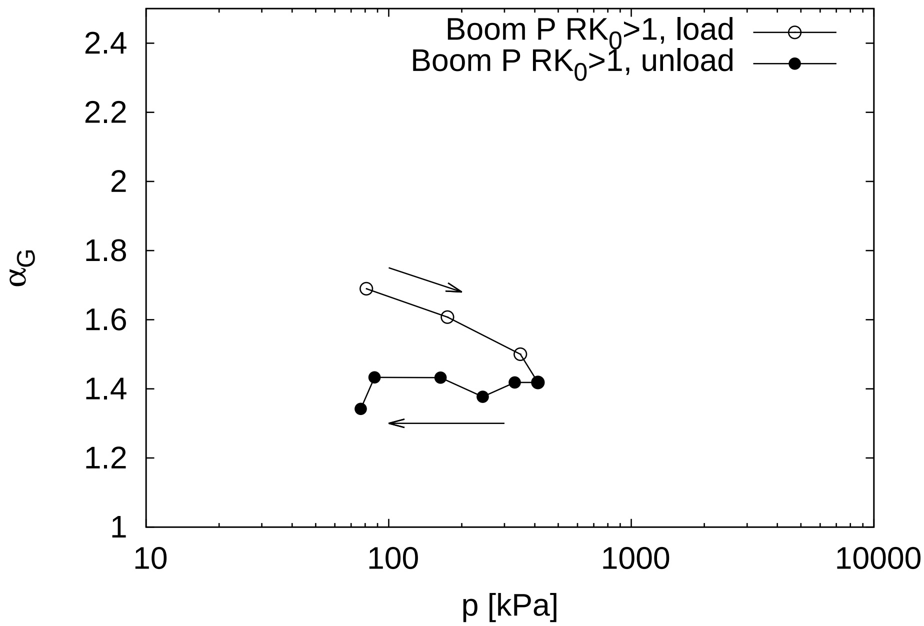

Figure 3: Development of stiffness anisotropy during $K_0 = 2$ loading and unloading of K_0 preconsolidated reconstituted clay (for data sources see Tab. 1).

K_0 compression (both datasets on Pisa clay). Some other data show more-or-less constant α_G during loading (Bangkok clay). Similarly, Chicago clay samples, which were obtained from different depths, show α_G, which is highly scattered but without any clear dependency on mean stress. Similar results to the "Chicago C NK_0" dataset were reported on different Chicago clay specimens by Kim and Finno [20].

Unexpectedly, three datasets (Panigaglia, Pietrafitta C and Taipei) show a decrease of α_G during K_0 loading. The Panigaglia and Pietrafitta C tests represent samples loaded under known K_0 conditions. The data on Taipei clay show α_G measurements on many samples from different depths K_0 reconsolidated to the *in-situ* vertical stresses. Clearly, stiffness anisotropy of Taipei clay decreases with sample depth, and stiffness anisotropy of Panigaglia and Pietrafitta C decreases during loading under K_0 conditions. In the case of Taipei clay, equivalent data on reconstituted soil are available (Fig. 1), where α_G increases with load. The decrease of α_G is thus probably caused by the effects of post-depositional structure in natural clay, which can degrade in compression and hinder the development of inherent anisotropy. The reason may be similar to the influence of artificial chemical treatment of natural soft clay by means of electro-osmosis, which has been discussed by Teng et al. [48].

Figure 5 shows the development of α_G during isotropic loading of soft natural clay (only data

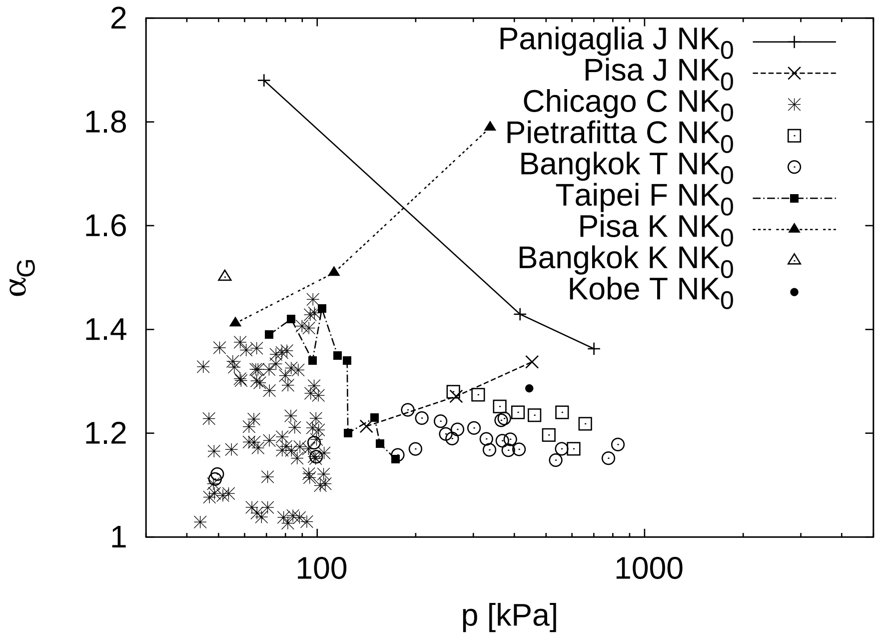

Figure 4: Development of stiffness anisotropy during oedometric loading of soft natural clays (for data sources see Tabs. 2 and 3).

on Shanghai clay are available). The anisotropy did not change substantially during isotropic loading. Certain decrease of α_G above $p = 100$ kPa may be observed, but this decrease may also be attributed to the measurement scatter. Relative insensitivity of α_G on mean stress during isotropic compression agrees with results of isotropically loaded samples of slightly K_0 overconsolidated reconstituted clay (see datasets Gault P RI, NSF Y RI and Kaolin K RI).

Figure 6 presents α_G evolution during K_0 unloading of natural soft clay samples, which were first loaded to vertical stresses higher than the stresses *in-situ*. All the samples consistently show substantial increase of α_G during K_0 unloading. The data on reconstituted clays indicated that unloading at constant K_0 (constant η) does not influence inherent stiffness anisotropy. α_G increase during K_0 unloading thus should be attributed to an increase in K_0 (decrease of η), rather than to a decrease of the vertical stress - it is thus a manifestation of stress-induced anisotropy.

Special type of tests described Landon and DeGroot [23]. They extracted undisturbed soil samples from different depths and measured their stiffness using portable bender elements, along with measurement of residual pore water pressures using suction probes. As the residual pore water pressure was very slow, their measurements reveal inherent soil anisotropy. Two soils (Boston Blue clay and Onsøy clay) exhibited increase of α_G with sampling depth, whereas

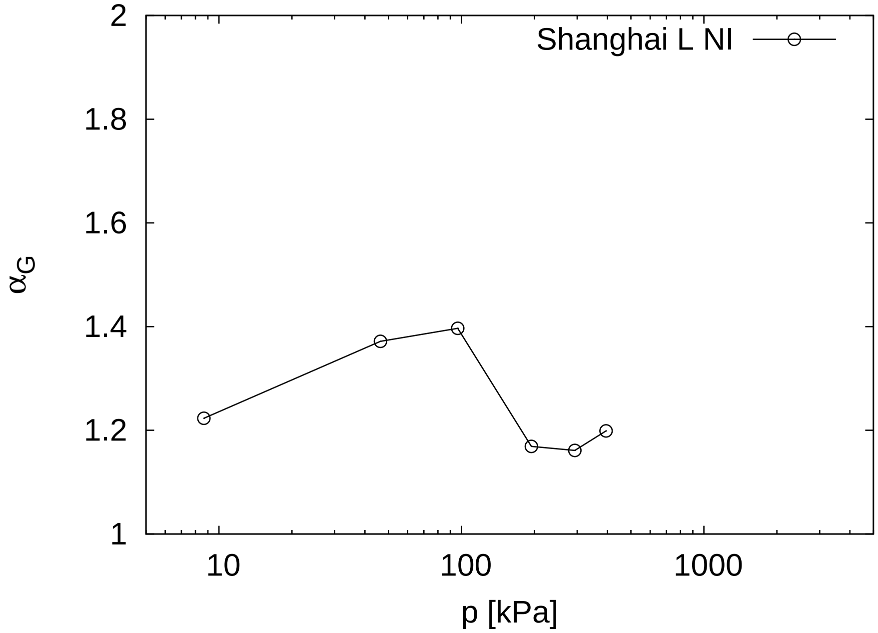

Figure 5: Development of stiffness anisotropy during isotropic loading of soft natural clays (for data sources see Tabs. 2 and 3).

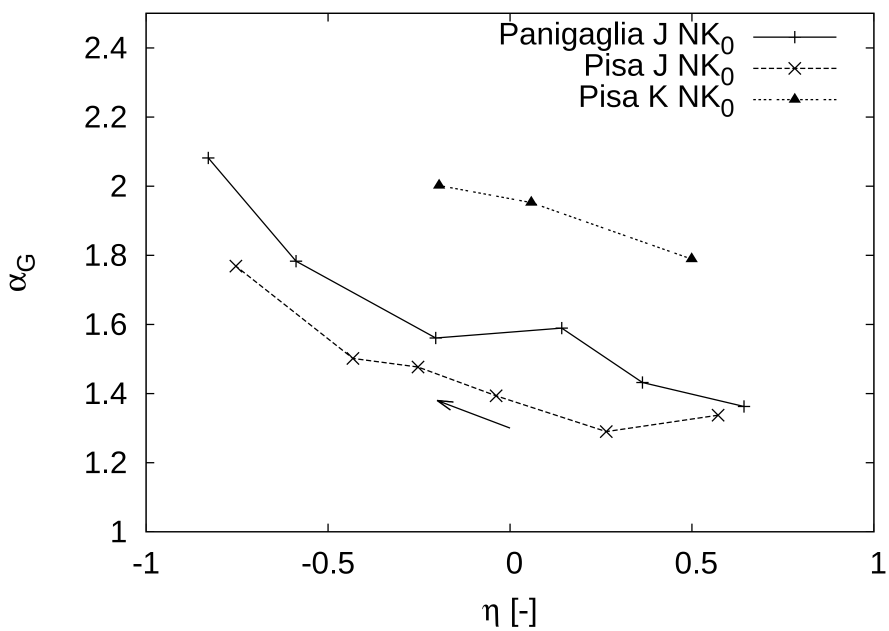

Figure 6: Development of stiffness anisotropy during oedometric unloading of K_0 consolidated soft natural clays (for data sources see Tabs. 2 and 3).

one soil (Burswood clay) did not show remarkable anisotropy. In fact, α_G of Burswood clay was even slightly lower than one, but this can probably be attributed to the experimental scatter caused by inaccuracies of measurements using portable bender element transducers.

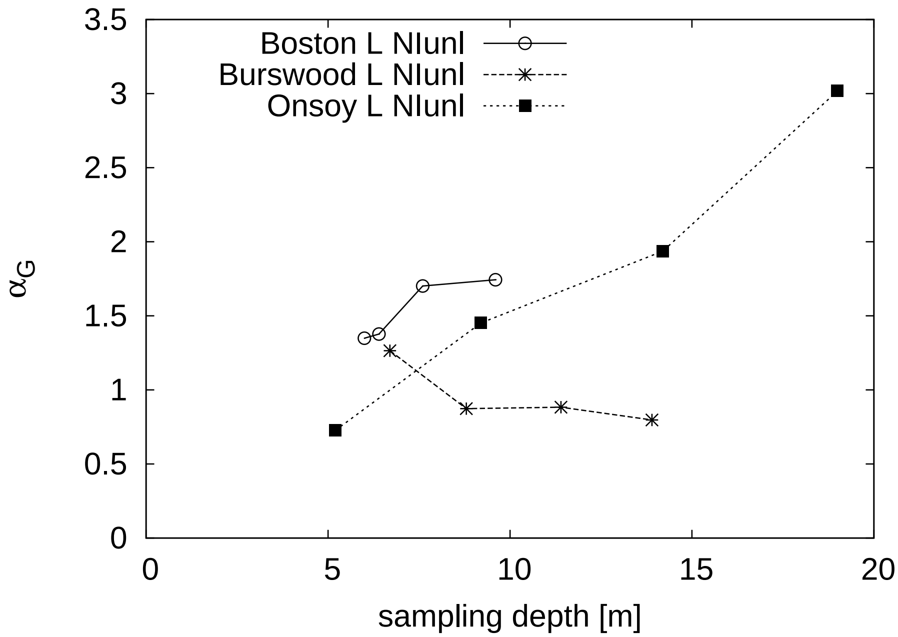

Figure 7: Stiffness anisotropy of different soft and stiff clays measured using portable bender elements on unloaded samples (for data sources see Tabs. 2 and 3).

5.3 Evolution of α_G of stiff sedimentary clays

This subsection summarises data on α_G evolution of stiff (highly overconsolidated) sedimentary clays. We first evaluate the data on oedometrically loaded samples. The data in Fig. 8, all represented in the form of graph of α_G vs. mean effective stress, were obtained using different experimental procedures. "London G" and "London N" data represent samples obtained from different depths reconsolidated to the estimated *in-situ* stress state (characterised by K_0, which decreases with increasing sample depth). These two datasets (obtained in the same laboratory at Imperial College, London) are consistent with each other, and indicate $\alpha_G \approx 2$ independently of sample depth. The α_G dependency on η is in Fig. 9; no clear dependency may be observed.

The datasets denoted as "Gault P" and "Gault L" were obtained in different way (see Tab. 4 for more details). The samples were first isotropically consolidated to the mean stress equal to the *in-situ* vertical effective stress, and then K_0 was increased by increasing the horizontal stress under constant vertical stress up to the estimated *in-situ* K_0 (2.1 and 2 respectively). The data in Figs. 8 and 9 were obtained during the K_0 increase phase. As the K_0 loading of highly overconsolidated clays does not substantially influence α_G (see results on reconstituted material), it is expected that the observed increase of α_G during K_0 increase is caused by the development of stress-induced anisotropy. This increase is, however, less substantial than in the case of soft natural clays (compare Figs. 9 and 6).

The last dataset in Fig. 8 represent the results of $K_0 = 2$ loading and unloading test on a single Boom clay sample. As K_0 is constant in this test, the stress induced anisotropy does not play a role in the data evaluation. Increase of mean stress leads to a slight increase of α_G. This is not in agreement with test on reconstituted soil, which showed α_G decrease during $K_0 > 1$ loading (Fig. 3).

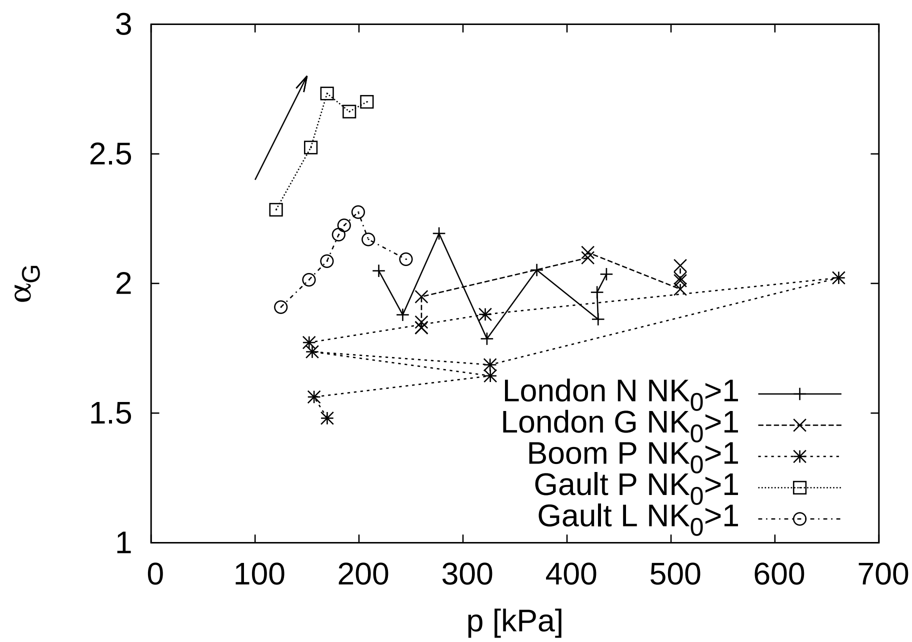

Figure 8: α_G dependency on mean stress of natural stiff clay samples under conditions of $K_0 > 1$ (for data sources see Tab. 4).

Figure 10 depicts the dependency of α_G on mean stress of natural stiff clays under isotropic stress state. The figure summarises results on samples from different depths (London N and London J), as well as single samples loaded to various stress levels (Boom P, London Y and Gault Y). In all cases, α_G appears to be independent of p.

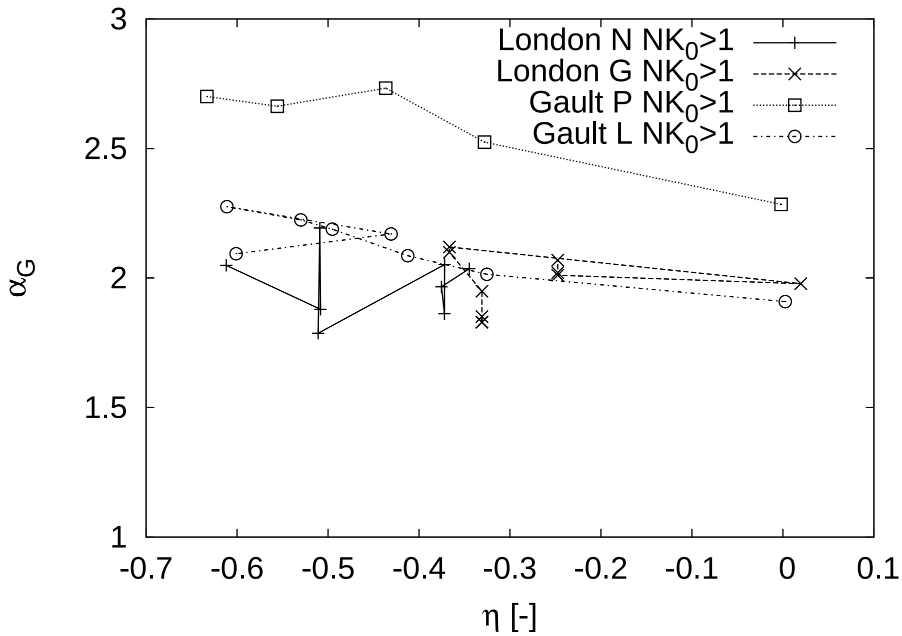

Figure 9: α_G dependency on η of natural stiff clays samples under conditions of $K_0 > 1$ (for data sources see Tab. 4).

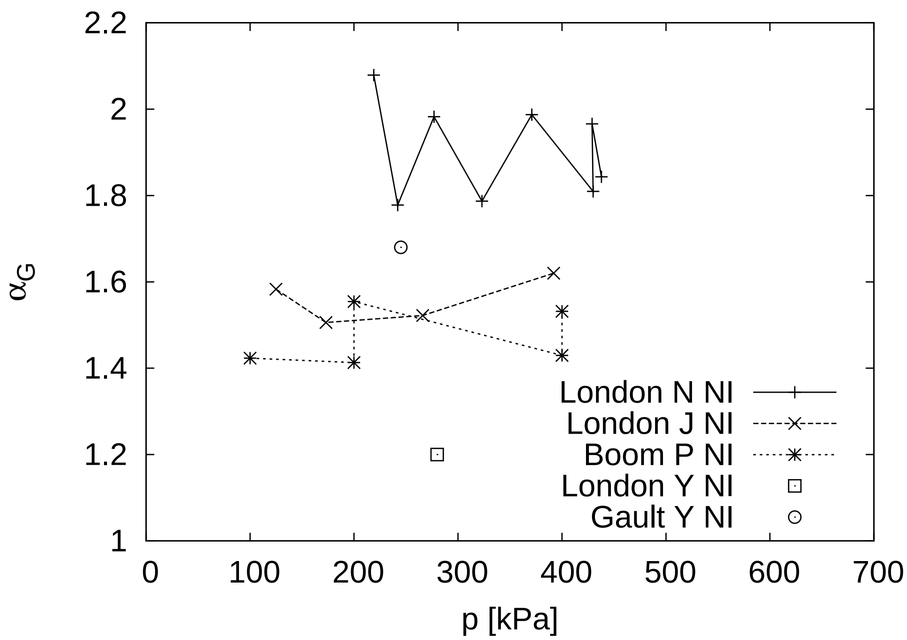

Figure 10: α_G dependency on mean stress of natural stiff clays samples under isotropic stress conditions (for data sources see Tab. 4).

6 Experimental evidence for the anisotropy exponents x_{GE} and $x_{G\nu}$

From the list of anisotropy parameters, α_G can be determined most reliably, as we can use bender element measurements of shear wave velocities. More difficult is the evaluation of α_E. Several studies are available in the literature only, which are applicable for the evaluation of the exponent x_{GE}. The α_E was measured in static loading tests using local strain measurements and not using wave propagation techniques as suggested in Sec. 3. The results and conclusions based on them are thus subject to experimental inaccuracies. All data available to the authors are summarised in Fig. 11. The data are scattered, but clearly the value of the exponent x_{GE} is in most cases higher than $x_{GE} = 0.5$ assumed by the Graham and Houlsby [14] model. An average value of the available measurements is approximately $x_{GE} \approx 0.8$.

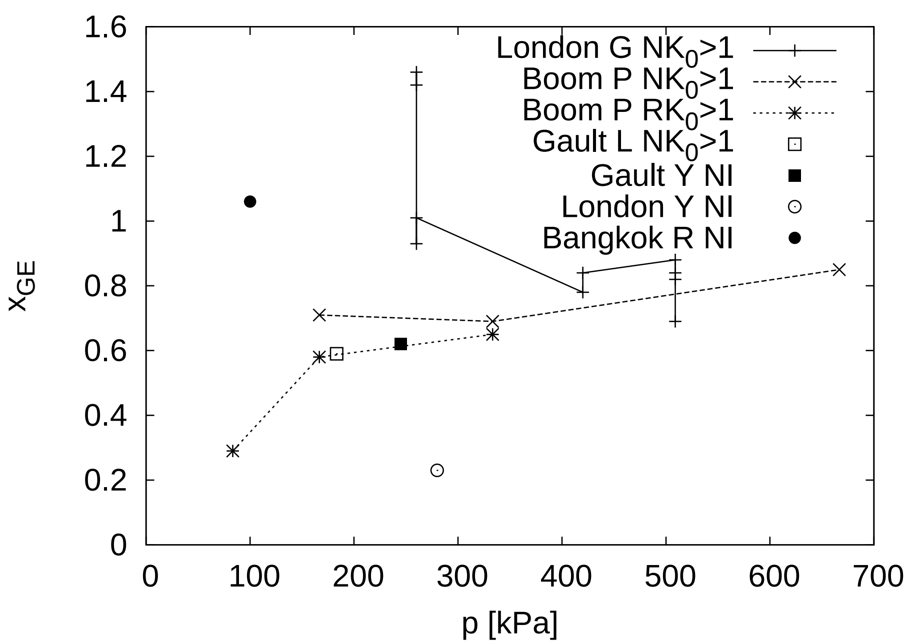

Figure 11: Dependency of the exponent x_{GE} on mean stress; all available measurements (for data sources see Tabs. 1 and 4).

While the exponent x_{GE} is difficult to estimate experimentally, evaluation of $x_{G\nu}$ is even more problematic, in the case wave velocity propagation methods are not used. The available experimental data on ν_{tp} and ν_{pp} are summarised in Fig. 12 (none of them is based on P-wave measurements). The data are very scattered, without any clear trend, and they do not allow to extract any information on the $x_{G\nu}$ value. In fact, in some cases (when one of the ν_{pp} and ν_{pt} is positive while the other is negative) $x_{G\nu}$ is undefined.

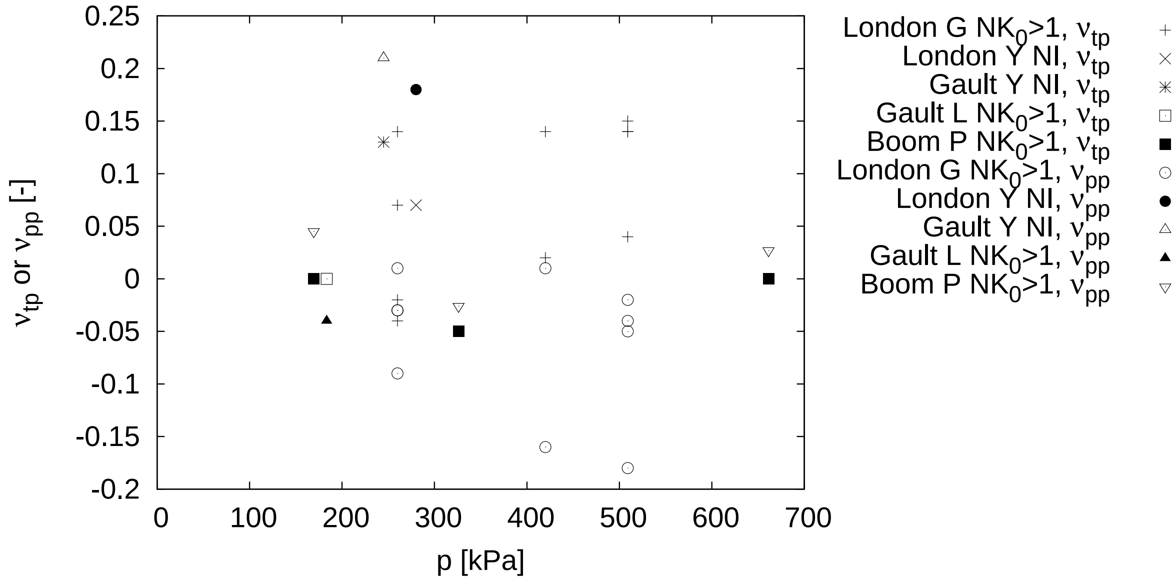

Figure 12: Poisson ratios ν_{tp} and ν_{pp} (for data sources see Tabs. 1 and 4).

7 A model for the very small strain stiffness anisotropy of sedimentary clays

The very small strain stiffness anisotropy is within the scope of the present paper described by means of α_G, x_{GE} and $x_{G\nu}$. It follows from Sec. 5 and 6 that the experimental knowledge on α_G, x_{GE} and $x_{G\nu}$ and their evolution with soil state is far from being complete. Nevertheless, the available information show some general trends. In this section, we will attempt to summarise them into a simple model. The model is restricted in its validity to triaxial stress conditions.

Here is the summary of formal findings on α_G evolution:

1. K_0 virgin loading of reconstituted clay with initially isotropic structure leads to a development of inherent stiffness anisotropy. Some soft natural clays show increase of α_G during K_0 compression consistently with the results on reconstituted clay, but some other show decrease of α_G. The latter trend is probably caused by the effects of post-depositional structure, which can degrade in compression.

2. Once the stiffness anisotropy has been developed, it may not easily be erased during isotropic or $K_0 > 1$ loading. Very mild change of anisotropy is observed once the soil reaches normally consolidated state; in an overconsolidated state and in unloading at constant stress ratio in particular, the α_G variability is negligible.

3. Soft clays (which are close to normally consolidated state) show substantial stress induced anisotropy. Decrease of η (increase of K_0) increases α_G.

4. Similar effect is observed in stiff clays (which are characterised by higher OCRs) but the effect of stress induced anisotropy is less pronounced.

The following relation is proposed which summarises the above properties.

$$\alpha_G = b_1 + b_2 \ln \frac{p_e}{p_r} + b_3 \left(K_0 - K_{0NC}\right) \left(\frac{p}{p_e}\right)^{b_4} \tag{36}$$

where b_1 to b_4 are parameters, p is mean effective stress, p_e is Hvorslev equivalent pressure, p_r is reference pressure 1 kPa and K_{0NC} is the value of K_0 in normally consolidated state.

Under K_0 normally consolidated conditions, K_0 is equal to K_{0NC} and p is equal to p_e and thus the first two terms of Eq. (36) are active only. They represent the contribution of inherent anisotropy. The equation prescribes linear increase (or decrease) of α_G with the logarithm of mean stress. The parameter b_2 controls the rate of α_G increase (positive b_2) or decrease (negative b_2) with p and the parameter b_1 represents the initial α_G. Once the soil is K_0 consolidated, p_e cannot be reduced substantially by subsequent loading. Eq. (36) thus predicts relative stability of inherent anisotropy. The model assumes that the current p_e was reached by one-dimensional compression, which is a reasonable assumption for natural clays; it is thus not applicable to isotropically or other than K_0 consolidated reconstituted clays.

The third term in Eq. (36) represents the contribution of stress-induced anisotropy. Here we assume that inherent and stress induced anisotropy effects are additive. The increase of α_G with K_0 is controlled by the parameter b_3. As OCR increases, the influence of the stress induced anisotropy is reduced, and this decrease is controlled by the parameter b_4.

Trends in predictions of Eq. (36) are demonstrated in Fig. 13. Figures 13a and 13b show the input data. K_0 compression and unloading curves of soft soil have been produced by a hypoplastic model by Mašín [29] with parameters $\varphi_c = 22°$, $\lambda^* = 0.128$, $\kappa^* = 0.015$, $N = 1.51$ and $\nu = 0.33$. Stress state of stiff clay was taken over from the "London N NK0>1" data with void ratio calculated such that $p_e = 1500$ kPa. Figures 13c and 13d show predictions by Eq. (36), with $b_1 = 0.6$, $b_2 = 0.11$, $b_3 = 0.7$ and $b_4 = 0.5$ (soft clay) and $b_1 = 0.85$, $b_2 = 0.11$, $b_3 = 0.7$ and $b_4 = 0.5$ (stiff clay). Experimental data on Pisa clay and London clay are also included in Figs 13c and 13d for demonstration purposes. The trends in α_G evolution are predicted properly by the proposed equation. In particular, the model predicts development of inherent stiffness anisotropy during K_0 compression and stress induced anisotropy in K_0 unloading of soft clay. Contrary, in stiff clay, α_G is almost independent of mean stress and η.

Note that Eq. (36) has been developed to demonstrate the conceptual outcomes of investigation described in this paper and is not aimed for engineering applications. The validity of Eq. (36) is restricted to the triaxial stress state and it assumes K_0 loading as the only process modifying the inherent stiffness anisotropy (in other words, it is assumed that any increase of p_e has been caused by K_0 compression). There are not enough data currently available to develop more general model of α_G evolution. An important simplification can be adopted in the case of stiff clays, where α_G does not vary substantially during loading process and for engineering applications it is reasonable to assume a constant value of α_G.

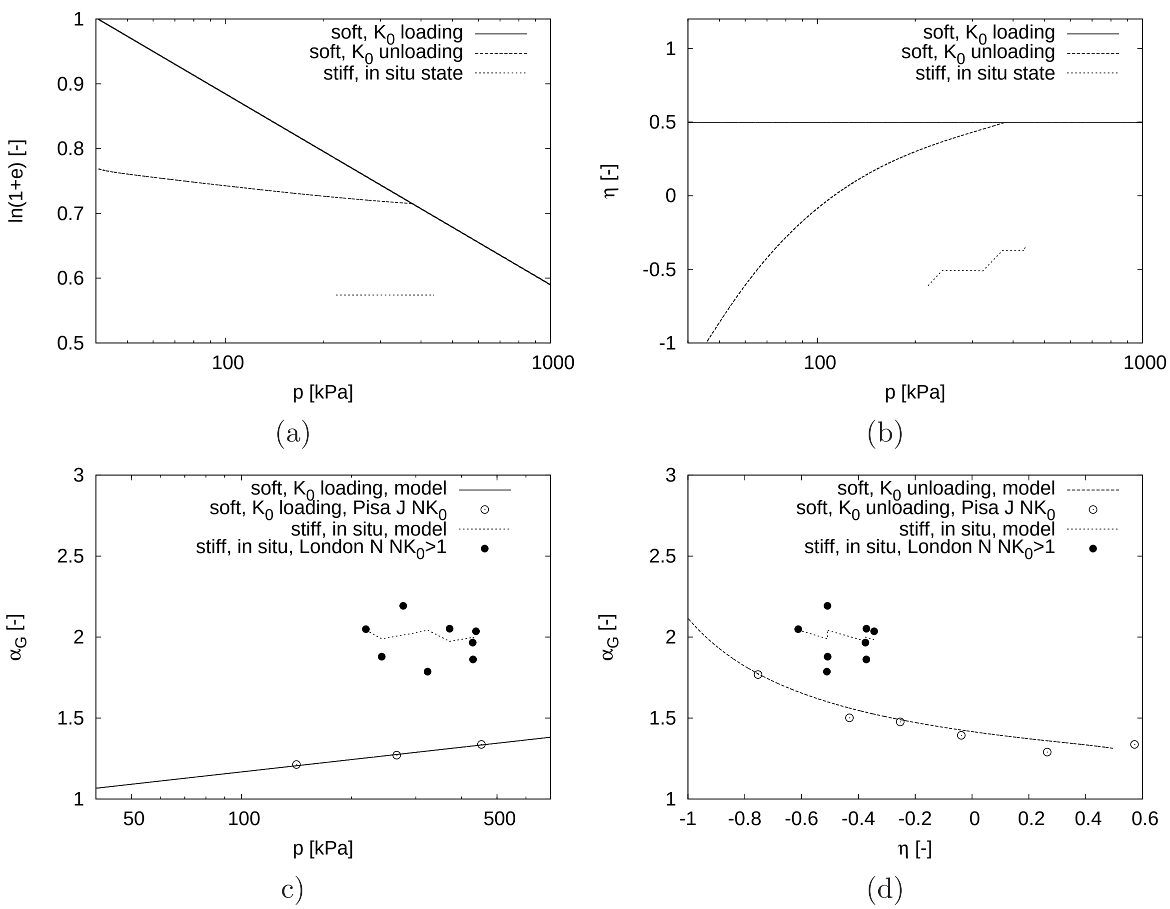

Figure 13: Input data (a,b) and predictions (c,d) of the conceptual model for evolution of shear stiffness anisotropy (for experimental data sources see Tabs. 2, 3 and 4).

While the experiments allowed us to interpret some general trends in the α_G evolution, much more complicated is the evaluation of the exponents x_{GE} and $x_{G\nu}$. In the case of absence relevant measurements, it is suggested to adopt $x_{GE} = 0.8$ value in the simulations, instead of $x_{GE} = 0.5$ implied by the Graham and Houlsby [14] model. $x_{GE} = 0.8$ is an approximate average value of available experimental data.

Measurement of Poisson ratios is extremely difficult, as is clear from highly scattered data from Fig. 12. The engineers would thus probably adopt the value $x_{G\nu} = 1$ of the Graham and Houlsby [14] model, although this value is not supported experimentally.

8 Summary and conclusions

A transversely isotropic elastic model has been rewritten in terms of the anisotropy coefficient α_G and anisotropy exponents x_{GE} and $x_{G\nu}$. Procedure for calibration of these variables using measurements of transversal and longitudinal wave velocities has been outlined. The coefficients have then be studied using experimental data from the literature. It has been shown that virgin oedometric loading of reconstituted clays leads to a development of inherent stiffness anisotropy, which cannot be easily reduced by subsequent loading. Some natural soft clays behave in a similar manner, but some show α_G decrease during K_0 compression, probably due to the effects of post-depositional structure, which can degrade in K_0 compression. Soft clays also show pronounced effect of stress-induced anisotropy, whose effect decreases with increasing overconsolidation ratio. α_G of stiff clays is stable and for engineering purposes it can be considered as constant throughout the loading process.

The value of the anisotropy exponent x_{GE} is more difficult to evaluate, but it is clear that it is typically higher than $x_{GE} = 0.5$ of the Graham and Houlsby [14] model. An average value of $x_{GE} = 0.8$ is recommended for practical applications in the case of absence of laboratory measurements. The most complicated is the evaluation of Poisson ratios, where the available data are extremely scattered and do not show any clear trends.

All the studied data are at axisymmetric stress conditions, where the axis of symmetry coincides with the axis of transverse isotropy. Development of stiffness anisotropy under general stress conditions is a complex matter as the response is no-more bound by the five-parameter transversely isotropic elasticity. It remains to be clarified in future research.

9 Acknowledgment

The research presented in this paper has been funded by the grant P105/12/1705 of the Czech Science Foundation.

References

[1] T. Addenbrooke, D. Potts, and A. Puzrin. The influence of pre-failure soil stiffness on the numerical analysis of tunnel construction. *Géotechnique*, 47(3):693–712, 1997.

[2] J. H. Atkinson. Non-linear soil stiffness in routine design. *Géotechnique*, 50(5):487–508, 2000.

[3] L. Callisto and S. Rampello. Shear strength and small–strain stiffness of a natural clay under general stress conditions. *Géotechnique*, 52(8):547–560, 2002.

[4] W. Cho and R. J. Finno. Stress-strain responses of block samples of compressible Chicago glacial clays. *Journal of Geotechnical and Geoenvironmental Engineering ASCE*, 136(1):178–188, 2010.

[5] J. Choo, Y.-H. Jung, and C.-K. Chung. Effect of directional stress history on anisotropy of initial stiffness of cohesive soils measured by bender element tests. *Soils and Foundations*, 51(4):737–747, 2011.

[6] C. R. I. Clayton. Stiffness at small strain: research and practice. *Géotechnique*, 61(1):5–37, 2011.

[7] C. R. I. Clayton and G. Heymann. Stiffness of geomaterials at very small strains. *Géotechnique*, 51(3):245–255, 2001.

[8] A. Ezaoui and H. Di Benedetto. Experimental measurements of the global anisotropic elastic behaviour of dry hostun sand during triaxial tests, and effect of sample preparation. *Géotechnique*, 57(7):621–635, 2009.

[9] J. N. Franzius, D. M. Potts, and J. B. Burland. The influence of soil anisotropy and K_0 on ground surface movements resulting from tunnel excavation. *Géotechnique*, 55(3):189–199, 2005.

[10] T. Fu-Chen. *Prediction of ground movement induced by excavation using the numerical method with the consideration of inherent stiffness anisotropy.* PhD thesis, National Taiwan University of Science and Technology, 2010.

[11] A. Gasparre. *Advanced laboratory characterisation of London Clay*. PhD thesis, University of London, Imperial College of Science, Technology and Medicine, 2005.

[12] A. Gasparre, S. Nishimura, N. A. Minh, M. R. Coop, and R. J. Jardine. The stiffness of natural London Clay. *Géotechnique*, 57(1):33–47, 2007.

[13] R. Giot, A. Giraud, T. Guillon, and C. Auvray. Three-dimensional poromechanical back analysis of the pulse test accounting for transverse isotropy. *Acta Geotechnica*, 7:151–165, 2012.

[14] J. Graham and G. T. Houlsby. Anisotropic elasticity of a natural clay. *Géotechnique*, 33(2):165–180, 1983.

[15] P. D. Greening and D. F. T. Nash. Frequency domain determinantion of G_0 using bender elements. *Geotechnical Testing Journal*, 27(3):288–294, 2004.

[16] M. J. Gunn. The prediction of surface settlement profiles due to tunnelling. In G. T. Houlsby and A. N. Schofield, editors, *Predictive soil mechanics: Proceedings of the Worth Memorial Symposium, London*, pages 304–316. Thomas Telford, London, 1993.

[17] M. Jamiolkowski, R. Lancellotta, and D. C. F. Lo Presti. Remarks on the stiffness at small strains of six Italian clays. In L. Jamiolkowski and L. Presti, editors, *Pre-failure Deformation Characteristics of Geomaterials*, pages 817–836. Balkema, Rotterdam, 1999.

[18] V. Jovičić and M. R. Coop. The measurement of stiffness anisotropy in clays with bender element tests in the triaxial apparatus. *Geotechnical Testing Journal*, 21(1):3–10, 1998.

[19] T. Kawaguchi, S. Yamashita, S. Kataoka, S. Shibuya, and S. Kawajiri. Inherent and induced anisotropy of three natural sedimentary clays reflecting on the elastic shear modulus. In S. E. Burns, P. W. Mayne, and J. C. Santamarina, editors, *Proc. 4^{th} International Symposium on Deformation Characteristics of Geomaterials, Atlanta*, pages 575–579, 2008.

[20] T. Kim and R. J. Finno. Anisotropy evolution and irrecoverable deformation in triaxial stress probes. *Journal of Geotechnical and Geoenvironmental Engineering ASCE*, 138(2):155–165, 2012.

[21] T.-C. Kung and C.-Y. Ou. Stress-strain characteristics of the Taipei silty clay at small strain. *Journal of the Chinese Institute of Engineers*, 27(7):1077–1080, 2004.

[22] R. Kuwano, T. M. Connolly, and J. Kuwano. Shear stiffness anisotropy measured by multi-directional bender element transducers. In L. Jamiolkowski and L. Presti, editors,

Pre-failure Deformation Characteristics of Geomaterials, pages 205–2012. Balkema, Rotterdam, 1999.

[23] M. M. Landon and D. J. DeGroot. Measurement of small strain shear modulus anisotropy on unconfined clay samples using bender elements. In *GeoCongress 2006: Geotechnical Engineering in the Information Technology Age, DOI: 10.1061/40803(187)20*. American Society of Civil Engineers, 2006.

[24] Q. Li. *Long-term settlement mechanisms of shield tunnels in Shanghai soft clay*. PhD thesis, The Hong Kong University of Science and Technology, 2013.

[25] Q. Li, C. W. W. Ng, and G. B. Liu. Determination of small-strain stiffness of Shanghai clay on prismatic soil specimen. *Canadian Geotechnical Journal*, 49:986–993, 2012.

[26] M. L. Lings, D. S. Pennington, and D. F. T. Nash. Anisotropic stiffness parameters and their measurement in a stiff natural clay. *Géotechnique*, 50(2):109–125, 2000.

[27] V. A. Lubarda and M. C. Chen. On the elastic moduli and compliences of transversely isotropic and orthotropic materials. *Journal of Mechanics of Materials and Structures*, 3(1):153–171, 2008.

[28] G. Mavko, T. Mukerji, and J. Dvorkin. *The Rock Physics Handbook: tools for seismic analysis of porous media*. Cambridge University Press, New York, 2^{nd} edition, 2009.

[29] D. Mašín. Clay hypoplasticity with explicitly defined asymptotic states. *Acta Geotechnica, DOI:10.1007/s11440-012-0199-y*, 2012.

[30] D. Mašín. Hypoplastic Cam-clay model. *Géotechnique*, 62(6):549–553, 2012.

[31] P. W. Mayne and F. H. Kulhawy. K_0–OCR relationships in soil. In *Proc. ASCE J. Geotech. Eng. Div.*, volume 108, pages 851–872, 1982.

[32] G. Mitaritonna, A. Amorosi, and F. Cotecchia. Elastic stiffness anisotropy of clay samples radially compressed along different stress ratio triaxial paths. In S. E. Burns, P. W. Mayne, and J. C. Santamarina, editors, *Proc.* 4^{th} *International Symposium on Deformation Characteristics of Geomaterials, Atlanta*, pages 589–595, 2008.

[33] C. W. W. Ng, Q. Li, and G. Liu. Measurements of small-strain inherent stiffness anisotropy of intact Shanghai soft clay using bender elements. *Chinese J. Geot. Eng.*, 35(7):150–156, 2013.

[34] W. W. C. Ng and E. H. Y. Leung. Determination of shear wave velocities and shear moduli of completely decomposed tuff. *Journal of Geotechnical and Geoenvironmental Engineering ASCE*, 133(6):630–640, 2007.

[35] A. Niemunis, C. E. Grandas Tavera, and L. F. Prada Sarmiento. Anisotropic visco-hypoplasticity. *Acta Geotechnica*, 4(4):293–314, 2009.

[36] S. Nishimura. *Laboratory study on anisotropy of natural London clay*. PhD thesis, University of London, Imperial College of Science, Technology and Medicine, 2005.

[37] D. S. Pennington, D. F. T. Nash, and M. L. Lings. Anisotropy of G_0 shear stiffness in Gault Clay. *Géotechnique*, 47(3):391–398, 1997.

[38] D. J. Pickering. Anisotropic elastic parameters for soil. *Géotechnique*, 20(3):271–276, 1970.

[39] K. Piriyakul. *Anisotropic Stress-Strain Behaviour of Belgian Boom Clay in the Small Strain Region*. PhD thesis, Ghent University, 2006.

[40] W. Ratananikom, S. Likitlersuang, and S. Yimsiri. An investigation of anisotropic parameters of Bangkok Clay from vertical and horizontal cut specimens. *Geomechanics and Geoengineering: An International Journal, DOI: 10.1080/17486025.2012.726746*, 8(1), 2013.

[41] G. P. Raymond. Discussion: Stresses and displacements in a cross-anisotropic soil, by l. barden. *Géotechnique*, 20(4):456–458, 1970.

[42] S. Salager, B. François, M. Nuth, and L. Laloui. Constitutive analysis of the mechanical anisotropy of Opalinus Clay. *Acta Geotechnica*, 8:137–154, 2013.

[43] M. Santagata, J. T. Germaine, and C. C. Ladd. Factors affecting the initial stiffness of cohesive soils. *Journal of Geotechnical and Geoenvironmental Engineering ASCE*, 131(4):430–441, 2005.

[44] S. Shibuya, S. C. Hwang, and T. Mitachi. Elastic shear moduli of soft clays from shear-wave velocity measurement. *Géotechnique*, 47(3):593–601, 1997.

[45] D. J. Shirley and L. D. Hampton. Shear-wave measurements in laboratory sediments. *The Journal of the Acoustical Society of America*, 63(2):607–613, 1978.

[46] A. J. M. Spencer. The formulation of constitutive equation for anisotropic solids. In J. P. Boehler, editor, *Mechanical behaviour of anisotropic solids*. Martinus Nijhoff Publishers, The Hague, 1982.

[47] S. Teachavorasinskun and P. Lukkanaprasit. Stress induced and inherent anisotropy on elastic stiffness of soft clays. *Soils and Foundations*, 48(1):127–132, 2008.

[48] F.-C. Teng, C.-Y. Ou, and S.-C. Chien. Investigations on stiffness anisotropy of soft clay with electro-osmosis chemical treatment. In Coutinho and Mayne, editors, *Geotechnical and Geophysical Site Characterisation 4*, pages 1551–1557. Taylor and Francis Group, 2013.

[49] G. Viggiani and J. H. Atkinson. Stiffness of fine–grained soil at very small strains. *Géotechnique*, 45(2):245–265, 1995.

[50] C. Wroth and G. Houlsby. Soil mechanics - property characterisation, and analysis procedures. In *Proc.* 11^{th} *Conf. Soil. Mech., San Francisco*, volume 1, pages 1–55, 1985.

[51] S. Yamashita, T. Hori, and T. Suzuki. Anisotropic stress-strain behavior at small strains of clay by triaxial and bender element tests. In P. V. Lade and T. Nakai, editors, *Proceedings of the Second Japan-U.S. Workshop on Testing, Modeling, and Simulation in Geomechanics, Kyoto, Japan; ASCE Geotechnical Special Publication 156*, pages 44–57, 2005.

[52] S. Yimsiri and K. Soga. Cross-anisotropic elastic parameters of two natural stiff clays. *Géotechnique*, 61(9):809–814, 2011.